Journal of Materials Chemistry A

V_2O_5 – Conductive Polymer Nanocables with Built-in Local Electric Field Derived from Interface Oxygen Vacancies for High Energy Density Supercapacitors

Journal:	*Journal of Materials Chemistry A*
Manuscript ID	TA-ART-04-2019-004264.R1
Article Type:	Paper
Date Submitted by the Author:	12-Jun-2019
Complete List of Authors:	Bi, Wenchao; Tongji University, Shanghai Key Laboratory of Special Microstructure Materials and Technology; University of Washington, Materials Science and Engineering, 406M Huang, Juanjuan; School of Physical Science and Technology, Lanzhou University; University of Washington, Materials Science and Engineering, 406M Wang, Ming-Shan; Southwest Petroleum University, School of Material Science and Engineering; University of Washington, Materials Science and Engineering, 406M Jahrman, Evan ; University of Washington, Department of Physics Seidler, Gerald ; University of Washington, Department of Physics Wang, Jichao; Tongji University, Wu, Yingjie; Monash University, Department of Material Science and Engineering Gao, Guohua; Tongji University, Pohl Institute of Solid State Physics Wu, Guangming; Tongji University, Shanghai Key Laboratory of Special Artificial Microstructure Materials and Technology, Pohl Institute of Solid State Physics Cao, Guozhong; University of Washington, Materials Science and Engineering

ARTICLE

V_2O_5 – Conductive Polymer Nanocables with Built-in Local Electric Field Derived from Interface Oxygen Vacancies for High Energy Density Supercapacitors

Received 00th January 20xx,
Accepted 00th January 20xx

DOI: 10.1039/x0xx00000x

Wenchao Bi [a, b], Juanjuan Huang [b, c], Mingshan Wang [b,d], Evan P. Jahrman [e], Gerald T. Seidler [e], Jichao Wang [a], Yingjie Wu [f], Guohua Gao [a]*, Guangming Wu [a]*, Guozhong Cao [b]*

Generating oxygen vacancies ($Vo^{¨}$) in vanadium pentoxide (V_2O_5) has been demonstrated as an effective approach to tailor its electrochemical properties. The present study investigates three different kinds of conductive polymers (CP = PPy, PEDOT, PANI) coated V_2O_5 nanofibers with $Vo^{¨}$ generated at the interface during polymerization process. Surface $Vo^{¨}$ form a local electric field and promote the charge transfer kinetics of the resulting $Vo^{¨}$-V_2O_5/CP nanocables, and the accompanying V^{4+} and V^{3+} may also catalyze the redox reactions and improve the supercapacitor performance. The differences and similarities of three different CP coatings have been compared and discussed, and related to their polymerization conditions and coating thickness. The dependence of $Vo^{¨}$ to form in the surface layer and in bulk have been elaborated and corresponding impacts on electrochemical properties and supercapacitor performance have also been investigated. $Vo^{¨}$-V_2O_5/CP can deliver a high capacity of up to 614 F g^{-1} at a current rate of 0.5 A g^{-1} and supercapacitors with $Vo^{¨}$-V_2O_5/CP demonstrated excellent cycling stability over 15000 cycles at a rate of 10 A g^{-1}.

Introduction

Supercapacitors (SCs) are appealing energy storage devices that have gained overwhelming attention due to their high power density, long cycling duration, safety, sustainability, and low-cost.[1-5] Rechargeable aqueous SCs will play a critical role in large-scale deployment of intermittent renewable energy sources, smart power grids, and electrical vehicles.[6-8] Due to the above advantages, substantial effort has been directed toward the development of SCs with higher energy density to meet ever-increasing requirements. In particular, much research has targeted electrode materials which greatly affect the electrochemical performance of SCs.[9-11] Transition metal oxides (TMOs) have promising applications in electrochemical energy storage due to their high theoretical specific capacitance and high energy density.[12, 13]

Vanadium pentoxide (V_2O_5), one such TMO, is appealing in electrochemical energy storage due to its high theoretical capacitance (2020 F g^{-1}), large voltage window (up to ~2.8 V), low cost, and abundance.[14, 15] Despite these advantages, the commercial viability of V_2O_5-based SCs is diminished by the low electrical conductivity of V_2O_5 (10^{-3} to 10^{-2} S cm^{-1}) and cycling instability, leading to unsatisfactory practical performance. Defects, especially oxygen vacancies ($Vo^{¨}$), could effectively improve the electrochemical performance of TMOs by adjusting their electronic structure while leaving the lattice as a whole largely unchanged.[16] Specifically, $Vo^{¨}$ can promote charge transfer kinetics with a larger interlayer spacing and allows the structure to be retained during cycling, and has thus been proposed to improve the specific capacitance and prolong the cycling duration of TMOs. [17-19] Conducting polymers (CPs) could also improve the electrical conductivity of V_2O_5, such as Poly(3,4-ethylenedioxythiophene) (PEDOT),[20] polypyrrole (PPy),[21] and polyaniline (PANI).[22] Gradient $Vo^{¨}$ on the V_2O_5 nanofiber (V_2O_5-NF) surface induced by PEDOT polymerization demonstrated much improved electrochemical properties and the resulting supercapacitor performance with facilitated charge transfer kinetics, and promoted redox reactions.[23] It was further revealed that the concentration of $Vo^{¨}$ at the V_2O_5-NF surface through tailoring the polymerization of PEDOT has an appreciable influence on the electrochemical properties and device performance.[24] Since all PPy, PANI and PEDOT belong to CPs and have been widely applied in supercapacitors, it is interesting to explore if all these three different kinds of CPs

[a] Shanghai Key Laboratory of Special Artificial Microstructure Materials and Technology, School of Physics Science and Engineering, Tongji University, Shanghai 200092, China.
[b] Department of Materials Science and Engineering, University of Washington, Seattle, WA 98195-2120, United States.
[c] MOE Key Laboratory for Magnetism and Magnetic Materials, School of Physical Science and Technology, Lanzhou University, Lanzhou 730000, China.
[d] The Center of New Energy Materials and Technology, School of Materials Science and Engineering, Southwest Petroleum University, Chengdu, Sichuan 610500, PR China
[e] Department of Physics, University of Washington, Seattle, WA 98195-1560, United States.
[f] Department of Material Science and Engineering, Monash University, Clayton, Victoria 3800, Australia

Electronic Supplementary Information (ESI) available: [Digital images, TG-DSC curves, XPS, HRTEM, CV and GCD curves]. See DOI: 10.1039/x0xx00000x

would generate $Vo^{¨}$ on the surface of V_2O_5-NF through a similar oxidative polymerization process, and how different CP coatings would work synergistically with $Vo^{¨}$ to influence the electrochemical properties and performance of V_2O_5-NF.

In this work, $Vo^{¨}$ are induced in the interface of V_2O_5-NF with different kinds of CPs (CP =PEDOT, PPy and PANI) to improve electrochemical performance of the obtained $Vo^{¨}$-V_2O_5/CP nanocables for high-performance supercapacitors. In the similar oxidative polymerization process, different thicknesses of CP coatings are obtained, and the induced $Vo^{¨}$ promote the charge transfer kinetics of resulting $Vo^{¨}$-V_2O_5/CP nanocables by forming a local electric field, and the accompanying V^{4+} and V^{3+} may also catalyze the redox reactions and improve the supercapacitor performance. The detailed relationships between the properties of CPs, the thickness of CP coatings, the overall concentration of $Vo^{¨}$, charge transfer kinetics, the electrochemical properties and supercapacitor performance are investigated and discussed.

Experimental section

Material characterizations

XRD patterns of as-prepared samples were obtained from X-ray diffractometer (XRD, Bruker D8 Advance, Germany) with a Rigaku D/max-C diffractometer and Cu-Kα (λ=0.15406 nm) radiation. The FTIR was performed using Bruker-TENSOR27 FTIR spectrometer from 400 to 4,000 cm^{-1}. TG-DSC analyses used SDT Q600 with temperature from 25 to 800 °C, at a heating rate of 10 °C min^{-1} in flowing air. Field emission scanning electron microscopy (FESEM, S-4800, Japan) and transmission electron microscopy (TEM, JEOLR2100, Japan) were employed to character the morphologies of all samples. XPS with Mg Kα radiation (hv = 1,253.6 eV) in PHI-5,000C ESCA system was used to examine the surficial vanadium oxidation states of all samples. X-ray absorption near edge structure (XANES) measurements (University of Washington) were performed at the vanadium K-edge with laboratory-based instrumentation to assess the bulk vanadium oxidation state distribution of all samples.[25, 26] The analysis and fitting used a previously reported methodology.[23]

Electrochemical measurements

The electrodes were made by painting a slurry (active materials, acetylene black and poly(vinylidene fluoride) (PVDF) in N-methylpyrrolidone (NMP) with a mass ratio of 8:1:1) onto a graphite paper current collector, and then dried under vacuum at 120 °C overnight. The electrodes are tested in a symmetric-electrode test cell and 1M Na_2SO_4 solution. Cyclic voltammogram (CV) and galvanostatic charge/discharge (GCD) and electrochemical impedance spectroscopy (EIS) were tested on a CHI660C (Chenhua) electrochemical working station (-1 to 1 V) [23] with the scan rates of CV from 5 to 10, 25, 50 and 100 mV s^{-1}, and the current densities of GCD from 0.5 to 1, 2.5, 5 and 10 A g^{-1}. The EIS was tested in the frequency from 10 mHz to 100 kHz with an AC voltage amplitude of 5 mV. The specific capacitance of each electrode (C, F g^{-1}) was obtained from the discharging process in GCD curves using the equation $C = 2\,I\,\Delta t\,/\,(m\,\Delta V)$, where I is the constant discharging current, m is the total mass of each electrode, Δt is discharging duration and ΔV is voltage window. Energy density (E, W h kg^{-1}) and power density (P, W kg^{-1}) in Ragone plots were calculated with the equations $E = (1/8)\,C\,(\Delta V)^2\,/3600$ and $P = E\,/\Delta t$, respectively.[24]

Preparation of $Vo^{¨}$-V_2O_5/CP nanocables

The synthesis of $Vo^{¨}$-V_2O_5/CP is schematically illustrated in **Fig. 1**. V_2O_5-NF is fabricated according to a reported method.[27] V_2O_5-NF is treated in vapored hydrochloric acid (HCl, 0.5 ml 36 wt%) in vacuum at room temperature for 1 h, as shown in step 1. In step 2, V_2O_5-NF is moved to another vacuum container and followed with 0.5 ml CP monomers (aniline, EDOT or pyrrole). Considering the different boiling points (Product SDS from Sigma-Aldrich, 760mm Hg) of pyrrole (129°C), aniline (184.1°C) and EDOT (193 °C), found in), the polymerization temperature of aniline and EDOT is kept at 80 ℃ for 6 h, while pyrrole polymerizes at room temperature for uniform polymerization. Then the monomers polymerize at the surface of V_2O_5-NF, forming a nanocable structure with $Vo^{¨}$ induced in the interface. The sample color changes from yellow to dark green (**Figure S1**). Then, $Vo^{¨}$-V_2O_5/CP nanocables are dried in vacuum at 120 ℃ overnight.

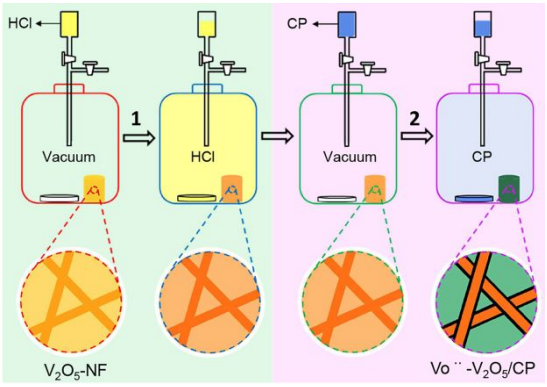

Fig. 1. Schematic diagram for the synthesis of $Vo^{¨}$-V_2O_5/CP (CP = PANI, PEDOT or PPy) nanocables.

Results and discussion

In the synthesis process, $Vo^{¨}$ are induced in the interface of $Vo^{¨}$-V_2O_5/CP nanocables. The polymerization process of CP is related to electron (e') loss and deprotonation (H^+). [28] As oxygen (O_o^x) in the V_2O_5 primitive lattice can donate electrons and generate $Vo^{¨}$ and O'', H_2O will form with O'' and H^+, and V_v^x in V_2O_5 receives electrons. Therefore, taking PPy for example, the possible reactions (1~4) are as follows.

$$n\,C_4H_5N - (2n-2)e' \rightarrow H(C_4H_2NH)_nH + (2n-2)\,H^+ \quad (1)$$

$$O_o^x = Vo^{¨} + O'' \quad (2)$$

$$2H^+ + O'' \rightarrow H_2O\ (g) \quad (3)$$

$$V_v^x + e' \rightarrow V_v',\ V_v' + e' \rightarrow V_v'' \quad (4)$$

Thus, the above reactions can be presented as follows.

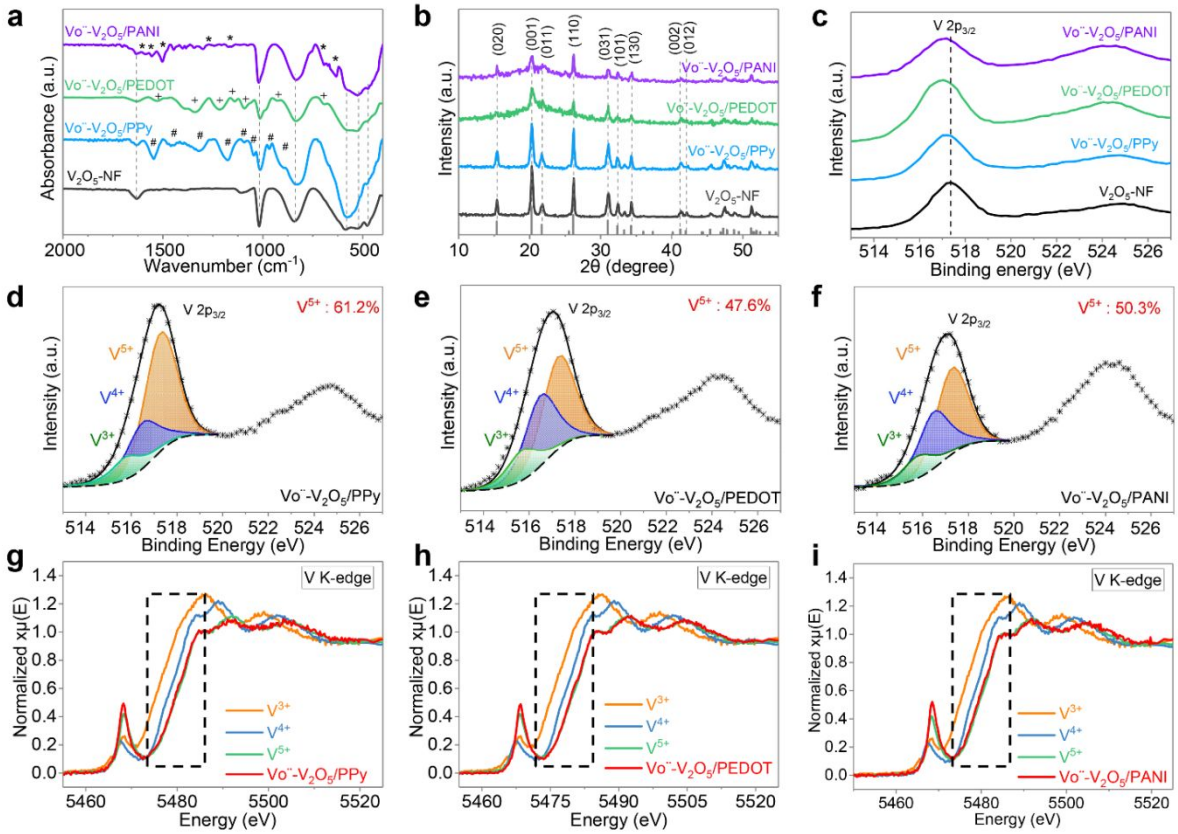

Fig. 2. (a) FTIR spectrum, (b) XRD patterns of Vo¨- V_2O_5/CPs and V_2O_5-NF. (c) V 2p peaks XPS spectrum of Vo¨- V_2O_5/CPs and V_2O_5-NF. (d, e, f) The decompositions of V $2p_{3/2}$ peak of Vo¨- V_2O_5/CPs. (g, h, i) The V K-edge XANES spectra of Vo¨- V_2O_5/CPs alongside empirical standards. The dashed box denotes the general vicinity of the V K-edge for these materials.

$$n\,C_4H_5\mathrm{N} + (2n-2)V_v^x + (n-1)\mathrm{O}_o^x \rightarrow \mathrm{H}(C_4\mathrm{H}_2\mathrm{NH})_n\mathrm{H} + (n-1)H_2\mathrm{O}\ (\mathrm{g}) + \mathrm{m}V_v^{x'} + (\mathrm{n}-1-\frac{1}{2}\mathrm{m})V_v^{x''} + (\mathrm{n}-1)\mathrm{Vo}^{\cdot\cdot} \quad (5)$$

Based on the above analysis, the concentration of Vo¨ is directly related to the polymerization process.

Fourier transform infrared (FT-IR) spectra (**Fig. 2a**) of all samples exhibit the characteristic bands of V_2O_5-NF with the stretching absorption modes of V=O bond (1022 cm^{-1}) and V-O-V bond (853, 520, and 483 cm^{-1}).[29] As for Vo¨-V_2O_5/PPy, the PPy is shown (marked with #) by C=C or C−C bonds in the pyrrole ring (1545 and 1460 cm^{-1}), in-plane deformations of C−H, C−N and N−H bond (1319, 1045, 1175, and 1093 cm^{-1}) and out-of plane deformations of C−H bonds (968 cm^{-1}).[30] For Vo¨-V_2O_5/PEDOT, the presence of PEDOT (marked with +) is shown by aromatic C=C and C-C bonds (1522 and 1397 cm^{-1}), C-O-C bonds (1207, 1143, and 1090 cm^{-1}), and C-S bonds (934, 833, and 692 cm^{-1}).[31] The main characteristic bands of PANI (marked with *) in Vo¨-V_2O_5/PANI are aromatic C=C and C=N bonds (1634, 1587, and 1502 cm^{-1}), C-N, C-H bonds (1300 and 1172 cm^{-1}), and the aromatic ring and out-of-plane deformation (692 and 633 cm^{-1}).[32, 33]

Thermogravimetry (TG) and differential scanning calorimetry (DSC) measurements in **Figure S2** show that the mass ratios of PPy, PEDOT and PANI in corresponding composites are ~18 %, ~27% and ~40%, respectively.[30] Compared with PEDOT, the larger percentage of PANI should be attributed to the lower boiling point and the smaller molecular weight (obtained from product SDS, Sigma-Aldrich) of aniline monomer (184.1°C, 93.1 g mol^{-1}) than EDOT monomer (193 °C, 142.2 g mol^{-1}). Although the pyrrole possesses a lower boiling points and a smaller molecular weight (129 °C, 67.1 g mol^{-1}) than aniline and EDOT, the higher reaction temperature of PANI (80 °C) and PEDOT (80 °C) than PPy (room temperature) would accelerate the polymerization.[34]

In **Fig. 2b**, X-ray diffraction (XRD) patterns display pure V_2O_5 phase (JCPDS No.85-0601) in all samples, suggesting unchanged crystalline information during the polymerization process. The broadened and lower intensity peaks in Vo¨-V_2O_5/CPs indicate the evolution of an amorphous phase, which might be caused by Vo¨ and CPs.

X-ray photoelectron spectroscopy (XPS) investigated the oxidation states of vanadium in the surface of Vo¨-V_2O_5/CPs. As shown in **Fig. 2c**, relative to V_2O_5-NF, the V $2p_{3/2}$ peaks of all Vo¨-V_2O_5/CPs move toward lower binding energies, indicating the reduction of Vo¨-V_2O_5/CPs. Considering the XRD patterns show a pure V_2O_5 phase, the reduction should be caused by Vo¨. The detailed decompositions of the V $2p_{3/2}$ peak show three peaks

for V^{5+}, V^{4+} and V^{3+} in **Fig. 2d, e, f** and **Figure S3.** The calculated concentration of V^{5+} in Vo¨-V_2O_5/PPy, Vo¨-V_2O_5/PEDOT, Vo¨-V_2O_5/PANI and V_2O_5-NF are 61.2%, 47.6%, 50.5% and 91.2%, respectively, and the corresponding concentration of Vo¨ (0.5V^{4+} and V^{3+}) are 26.0%, 34.2%, and 31.9%. Thus, the Vo¨ are induced in Vo¨-V_2O_5/CPs by polymerization of PPy, PEDOT and PANI. Further examination of the oxidation state of vanadium atoms in the system was accomplished with X-ray absorption near edge structure (XANES) measurements. These measurements provided insight into Vo¨ concentrations in the bulk of each sample and complemented the XPS results which only characterize the shallow surface of each samples and might be less representative of speciation in the bulk, especially with thick CP coatings at the surface of V_2O_5-NF. The V K-edge XANES spectra of Vo¨-V_2O_5/CPs are shown with respect to commercial V_2O_3, VO_2 and V_2O_5, which served as empirical standards.[23] The early stages of an edge shift are observed in the XANES spectra of Vo¨-V_2O_5/PPy (**Fig. 2g**) Vo¨-V_2O_5/PEDOT (**Fig. 2h**) and Vo¨-V_2O_5/PANI (**Fig. 2i**), respectively. As an edge shift to lower photon energies corresponds to reduction of the probed element, this suggests Vo¨ are present in Vo¨-V_2O_5/CPs, which is consistent with XPS and XRD analysis. However, the general agreement between the Vo¨-V_2O_5/CPs and the V_2O_5 spectra reveals the bulk of the V atoms remain in V^{5+}. Indeed, fitting results show a smaller percentage of Vo¨ (0.2 % for Vo¨-V_2O_5/PPy, 1.3% for Vo¨-V_2O_5/PEDOT and 5.4% for Vo¨-V_2O_5/PANI, respectively) than XPS results, confirming the near-surface modification of Vo¨. Moreover, the overall concentration of Vo¨ is generally consistent with the corresponding CP content from above TG results.

Scanning electron microscopy (SEM) and Transmission electron microscopy (TEM) images of Vo¨-V_2O_5/CPs show that V_2O_5-NF is coated homogeneously by ~6.7 nm PANI layer (**Fig. 3a,d,g**), ~5.0 nm PEDOT layer (**Fig. 3b,e,h**), ~3.5 nm PPy layer (**Fig. 3c,f,i**), respectively. This thickness of CP shell is roughly consistent with the above mass ratios. The even distributions of CP coatings are visually confirmed by High-angle annular dark-field scanning transmission electron microscopy (HAADF-STEM) images and corresponding element mappings, where the characteristic elements of CPs distribute uniformly, as shown in **Fig. 3m, n, o**. In **Fig. 3j**, further characterizations from Inverse Fast Fourier Transform (IFFT) of a High-Resolution TEM (HRTEM) image demonstrates dislocations with blurred lattice fringes in Vo¨-V_2O_5/PANI with an expanded interplanar spacing ranging from 5.93 to 6.29 Å (standard parameter is 5.76 Å), corresponding to the (020) crystal planes of V_2O_5. Moreover, the distorted lattice fringes are readily apparent and arise from Vo¨ which cause the skewing of vanadium atoms around the Vo¨ in V_2O_5. Similarly, the interplanar spacing of the (011) crystal planes of V_2O_5 in Vo¨-V_2O_5/PEDOT increases from 4.09 Å (standard parameter) to 4.25 Å in **Fig. 3k**, and that of (020) planes in Vo¨-V_2O_5/PPy is between 5.76 and 5.84 Å in **Fig. 3l**. Detailed information is shown in **Figure S4.** These IFFT images directly evidence the existence of Vo¨ in Vo¨-V_2O_5/CPs. Based

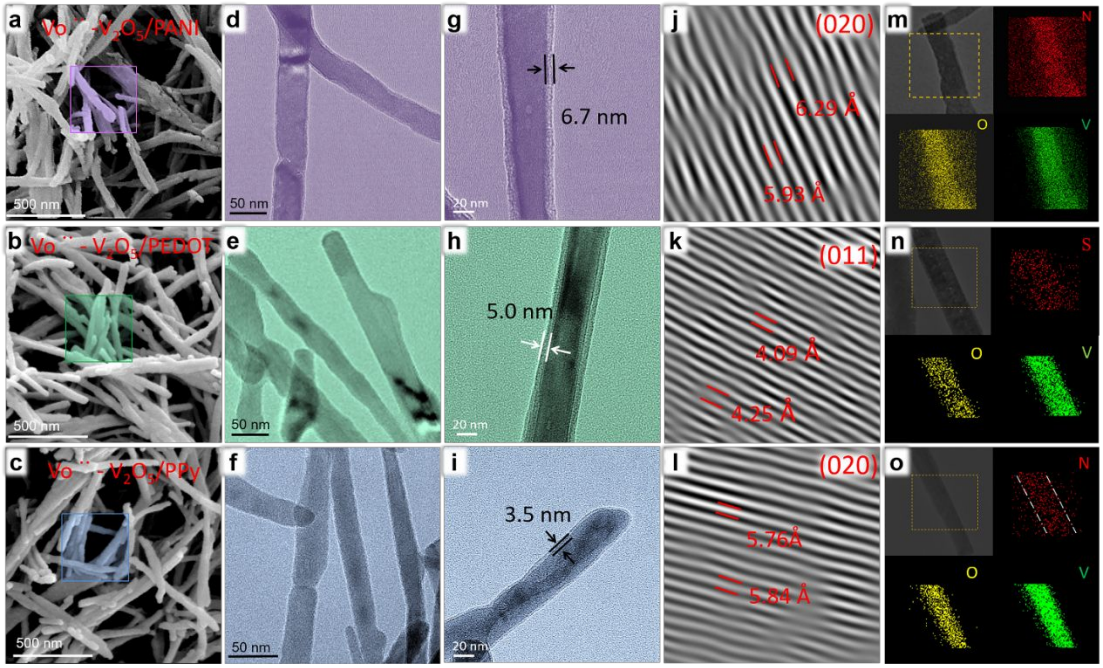

Fig. 3. (a, b, c) SEM images, (d, e, f, g, h, i) TEM images, (j, k, l) IFFT images, (n, m, o) HAADF-STEM images and corresponding element mappings of Vo¨-V_2O_5/CPs.

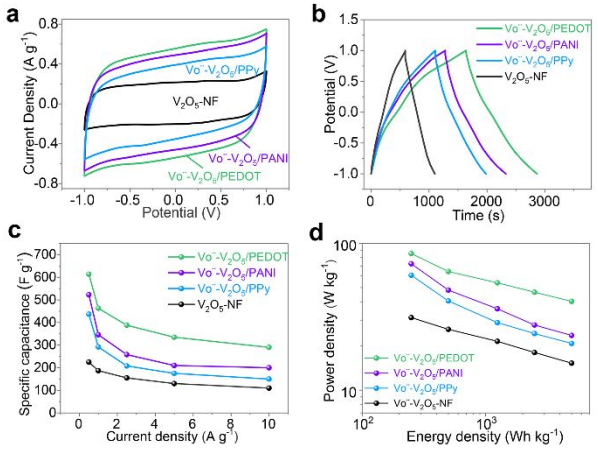

Fig. 4. (a) CV curves of Vo¨-V_2O_5/CPs and V_2O_5-NF at a scan rate of 5 mV s^{-1}. (b) GCD curves of Vo¨-V_2O_5/CPs and V_2O_5-NF at current density of 0.5 A g^{-1}. (c) Specific capacitances of Vo¨-V_2O_5/CPs and V_2O_5-NF under different current densities. (d) Ragone plots of Vo¨-V_2O_5/CPs and V_2O_5-NF.

on all the above structural and morphology analysis, it is clear that Vo¨ are generated in Vo¨-V_2O_5/CPs by PANI, PEDOT and PPy coatings.

Electrochemical potential of Vo¨-V_2O_5/CPs is evaluated using symmetrical double-supercapacitors (1 M Na_2SO_4 aqueous solute). The supercapacitive storage behavior is initially investigated by using cyclic voltammetry (CV). In **Fig. 4a** and **Figure S5**, CV curves of all samples appear with nearly rectangular shapes. This reveals excellent reversible redox capacities although without redox peaks, which is widely accepted as a result of the fast, reversible successive multiple surface redox reactions.[35] Compared with other samples, Vo¨-V_2O_5/PEDOT possesses a larger voltammogram area, indicating higher supercapacitive performance (**Fig. 4a**). Consistently, GCD curves of Vo¨-V_2O_5/CPs are nearly linear and symmetric under various current densities (**Figure S6**). The specific capacitances of Vo¨-V_2O_5/PEDOT (614 F g^{-1}), Vo¨-V_2O_5/PANI (523 F g^{-1}) and Vo¨-V_2O_5/PPy (437 F g^{-1}) are obviously superior to V_2O_5-NF (225 F g^{-1}) at 0.5 A g^{-1} (**Fig. 4b**). Vo¨-V_2O_5/CPs show larger specific capacitances than V_2O_5-NF even at a large current density of 10 A g^{-1}, as shown in **Fig. 4c**. When the power density is 2500 W kg^{-1}, the energy densities of Vo¨-V_2O_5/PEDOT, Vo¨-V_2O_5/PANI, Vo¨-V_2O_5/PPy and V_2O_5-NF are 85, 73, 61 and 31 W h kg^{-1}, respectively (**Fig. 4d**). The enhancement in the capacitance may be attributed to interface modifications of Vo¨ and CP shells, which will be further explored in the following text.

The role of Vo¨ in promoting charge transfer kinetics during the charging and discharging processes was firstly analyzed. **Fig. 5a** shows the crystal structure of V_2O_5 and images viewed along [010] and [001] directions. There are three kinds of vacancy sites in V_2O_5 according to the type of oxygen, including vanadyl oxygen (site 1), bridge oxygen (site 2) and chain oxygen (site 3), as shown in **Fig. 5b.** As the vanadyl oxygen (site 1) has been reported as the easiest site to generate Vo¨,[36] the following further analysis will focus on Vo¨ located at site 1. With skewing of vanadium atoms around the Vo¨ sites, which was observed as dislocations in above IFFT images, the charge distribution around Vo¨ sites is off balance in V_2O_5 plane, forming a positive region in the Vo¨ center and a corresponding negatively charged area around Vo¨. In the discharging process, as illustrated in **Fig. 5c**, due to the imbalanced charge distribution, an extra electric field forms with a direction from the non-Vo¨ area to the negatively charged region, and Na^+ ions in the electrolyte will be attracted by Coulombic force and move to the negatively charged region around the Vo¨. When it is fully discharged, the negatively charged area will be electrically neutral. In the

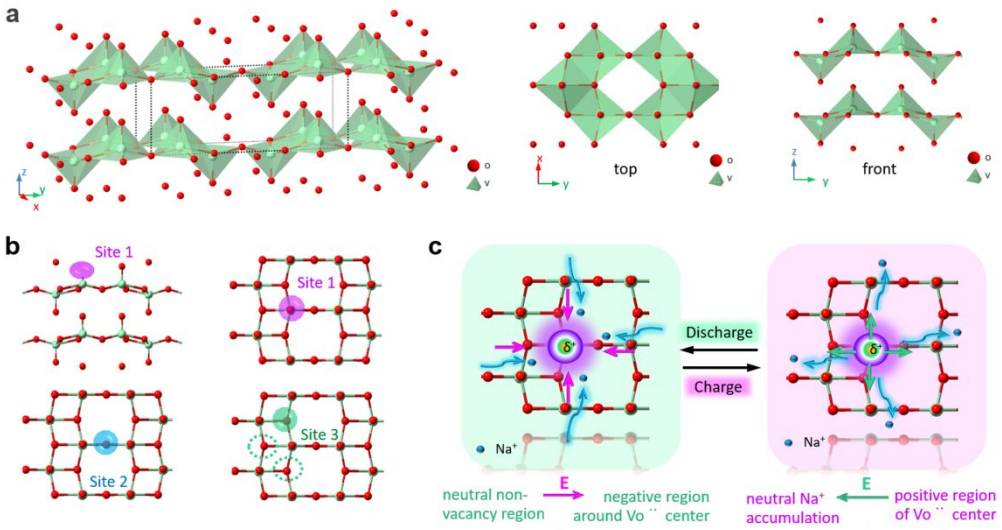

Fig. 5. (a) The crystal structure of V_2O_5 along [010] and [001]. (b) The three kinds of sites for Vo¨ in V_2O_5 bulk structure. (c) Schematic illustration of the enhanced ionic transfer kinetics around Vo¨ by forming a local electric field (E).

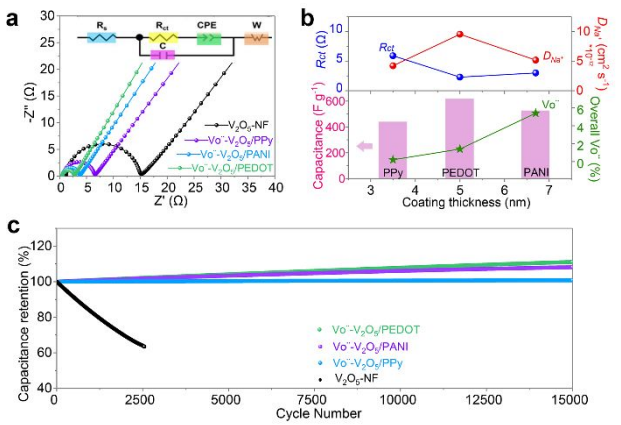

Fig. 6. (a) Nyquist plots of Vo¨-V_2O_5/CPs and V_2O_5-NF. (b) Relationships between the coating thickness, *Rct*, D_{Na+}, overall Vo¨ concentrations and the specific capacitances of Vo¨-V_2O_5/CPs. (c) Cycling performance of Vo¨-V_2O_5/CPs and V_2O_5-NF at 10 A g^{-1}

charging process, a local electric field forms with the direction from the positive Vo¨ center to the neutral Na^+ accumulation region, and the corresponding Coulombic forces will accelerate the migration of Na^+ ions away from the Vo¨ center. Thus, the ionic transfer dynamics in V_2O_5-NF is enhanced due to the local electric field caused by Vo¨, which was reported in Li-ion batteries as well.[37]

The kinetic reasons behind the high specific capacitances were further studied by electrochemical impedance spectroscopy (EIS). As shown in **Fig. 6a**, the interfacial charge transfer resistance (*Rct*) of Vo¨-V_2O_5/PPy (5.9 Ω), Vo¨-V_2O_5/PEDOT (2.3 Ω) and Vo¨-V_2O_5/PANI (3.0 Ω) are smaller than that of V_2O_5-NF (8.4 Ω), which suggests enhanced electronic transfer. The ion diffusion coefficients were calculated according to the formula[38]:

$$D = \frac{R^2 T^2}{2 A^2 n^4 F^4 C^2 {\sigma_w}^2} \quad (6)$$

The calculated Na^+ ion diffusion coefficients in all three Vo¨-V_2O_5/CPs are summarized in **Table S1**. All Vo¨-V_2O_5/PPy ($4.12*10^{-12}$), Vo¨-V_2O_5/PEDOT ($9.54*10^{-12}$ cm^2 s^{-1}) and Vo¨-V_2O_5/PANI ($5.17*10^{-12}$) show higher diffusion coefficient values than V_2O_5-NF ($2.51*10^{-12}$ cm^2 s^{-1}). The excellent specific capacitance of Vo¨-V_2O_5/CPs is likely attributed to improved charge transfer kinetics due to the synergistic combination of CP coatings and Vo¨. Vo¨ provide void sites to accept/donate electrons and cause a local electric field to enhance the Na^+ ion transfer dynamics (discussed above). The accompanied V^{4+} and V^{3+} would also exert catalytic effects to promote the redox reactions and lead to enhanced capacitance.[39] Moreover, CP coatings provide short and highly conductive pathways for rapid charge transfer, synergistically facilitating the charge storage and improving the specific capacitance. The synergistic effects of CP coating and Vo¨ were further proved, taking Vo¨-V_2O_5/PANI for example, by physically mixing V_2O_5-NF and commercial PANI. The obtained m-V_2O_5/PANI composite (without Vo¨) delivers a higher capacitance (312 F g^{-1}) than V_2O_5-NF (225 F g^{-1}), but much lower than Vo¨-V_2O_5/PANI (523 F g^{-1}) at 0.5 A g^{-1}. (The details can be found in **Figure S7**, supporting information.)

Fig. 6b shows that Vo¨-V_2O_5/PEDOT electrode possess a larger D_{Na+} value and a smaller *Rct* value ($9.54*10^{-12}$ cm^2 s^{-1}, 2.3 Ω) than Vo¨-V_2O_5/PANI ($5.17*10^{-12}$ cm^2 s^{-1}, 3.0 Ω) and Vo¨-V_2O_5/PPy ($4.12*10^{-12}$ cm^2 s^{-1}, 5.9 Ω), and the specific capacitance of Vo¨-V_2O_5/PEDOT (614 F g^{-1}) is higher than that of Vo¨-V_2O_5/PANI (523 F g^{-1}) and Vo¨-V_2O_5/PPy (437 F g^{-1}). This suggests that Vo¨-V_2O_5/PEDOT is most favorable for electrolyte ionic diffusion at the electrode-solution interface and electronic transfer, and thus leads to the most efficient charge storage among Vo¨-V_2O_5/CPs. Interestingly, the overall concentration of Vo¨ in Vo¨-V_2O_5/PEDOT (1.3%) is larger than that in Vo¨-V_2O_5/PPy (0.3%), but smaller than that in Vo¨-V_2O_5/PANI (5.2%). This can be explained that, besides the Vo¨, the CP coating synergistically improve to the charge transfer kinetics of Vo¨-V_2O_5/CPs. Theoretically, the electrical resistance (*R*) is related to electrical conductivity (σ), cross sectional area (A) and length (*L*), according to the electrical resistance formula $R=L/\sigma A$. With the different thickness of PPy (3.5 nm), PEDOT (5.0 nm) and PANI (6.7 nm), and the reported σ values of PEDOT (300~500 S cm^{-1}), PANI (0.1~5 S cm^{-1}) and PPy (10~50 S cm^{-1}),[40] the *R* value was estimated (**Table S2,** supporting information), and shows that the calculated *R* of Vo¨-V_2O_5/PEDOT (17~28 Ω/nm) is smaller than that of Vo¨-V_2O_5/PANI (1239~61941 Ω/nm) and Vo¨-V_2O_5/PPy (247~1237 Ω/nm). Thus, the combination of high electrical conductivity of PEDOT and Vo¨ leads to a high specific

	Vo¨-V_2O_5/PPy	Vo¨-V_2O_5/PEDOT	Vo¨-V_2O_5/PANI
Monomer's molecular weight (g mol^{-1})	67.1	142.2	93.1
Monomer's boiling point (°C)	129	193	184
Reaction temperature (°C)	25	80	80
Mass content	18 %	27%	**40%**
Coating thickness (nm)	3.5	5.0	**6.5**
Surface Vo¨ (XPS)	26.0%	34.2%	31.9%.
Overall Vo¨ (XANES)	0.2%	1.3%	**5.4%**
Rct (Ω)	5.9	**2.3**	3.0
D_{Na+} (cm^2 s^{-1})	$4.12*10^{-12}$	**$9.54*10^{-12}$**	$5.17*10^{-12}$
$R=L/\sigma A$ (Ω nm^{-1})	247~1237	**17~28**	1239~61941
σ (S cm^{-1})	10~50	300~500	0.1~5
Specific capacitance (F g^{-1})	437	**614**	523

Table 1. The related data of Vo¨-V_2O_5/CPs, including reaction temperature, physical and electrochemical properties, and resulting supercapacitor performance.

capacitance of $Vo^{¨}$-V_2O_5/PEDOT. That means both the CP type and $Vo^{¨}$ concentration should be considered to improve the electrochemical performance of V_2O_5.

The cycling performance was tested at 10 A g^{-1}, as shown in **Fig. 6c.** After 15000 cycles, $Vo^{¨}$-V_2O_5/PEDOT, $Vo^{¨}$-V_2O_5/PANI and $Vo^{¨}$-V_2O_5/PPy show 111%, 108% and 101% capacitance retention, respectively. The excellent cyclability can be attributed to positively charged $Vo^{¨}$ which balance the strain and stress from adjacent layers and inhibit the structural collapse of V_2O_5,[16] as well as the CP shells which protect the V_2O_5 core during the cycling process.[30] As the electric field drives surface-distributed $Vo^{¨}$ to immigrate and distribute homogeneously, more V^{5+} becomes accessible at the surface region of samples for redox reactions, leading to an increased capacitance.[41] The wetting and electro-activation from electrolyte might also increase the specific capacitance of electrodes during cycling process.[42] The stability of $Vo^{¨}$-V_2O_5/CP is superior to other SCs based on V_2O_5/PPy networks (81% capacitance retention after 1000 cycles),[21] V_2O_5/PPy (83% capacitance retention 2000 cycles),[30] V_2O_5/PEDOT/MnO_2 (94% capacitance retention after 3000 cycles), and V_2O_5/PANI nanowires (92 % capacitance retention after 5000 cycles).[33]

Conclusions

Oxygen vacancies ($Vo^{¨}$) were generated in the near surface region of $Vo^{¨}$-V_2O_5/CPs (CP = PANI, PEDOT, PPy) through the polymerization of CPs, and $Vo^{¨}$ formed a local electric field in the interface between V_2O_5-NF and CP coating. During charging and discharging processes, the local electric field promoted ion/electron transport, leading to enhanced charge transfer kinetics. The presence of V^{4+} and V^{3+} may catalyze the redox reactions and thus further enhances the electrochemical properties of $Vo^{¨}$-V_2O_5/CPs. CP shells provided conductive charge transfer pathways to synergistically optimize the charge storage properties. As a result, $Vo^{¨}$-V_2O_5/CP based supercapacitors delivered high specific capacitances up to 614 F g^{-1} and excellent cycling stability over 15000 cycles. It seems that both $Vo^{¨}$ and the nature of CPs has significant impact on the electrochemical properties and device performance.

Conflicts of interest

There are no conflicts to declare.

Acknowledgements

This work is supported financially in part by the National Natural Science Foundation of China (Granted No. U1503292, No. 51872204), the Fundamental Research Funds for the Central Universities, and the National Key Research and Development Program of China (Granted No. 2017YFA0204600). The work is also supported in part by the National Science Foundation (1803256). WCB was supported by the China Scholarship Council (CSC) for studying at the University of Washington. EPJ was supported by a subcontract from the National Institute of Standards and Technology. Opinions, recommendations, findings, and conclusions presented in this manuscript and associated materials does not necessarily reflect the views or policies of NIST or the United States Government.

Notes and references

1. T. Qin, B. Liu, Y. Wen, Z. Wang, X. Jiang, Z. Wan, S. Peng, G. Cao and D. He, *J. Mater. Chem. A*, 2016, **4**, 9196-9203.
2. L. Q. Mai, A. Minhas-Khan, X. Tian, K. M. Hercule, Y. L. Zhao, X. Lin and X. Xu, *Nat. Commun.*, 2013, **4**, 2923-2930.
3. G. Zhu, L. Yang, W. Wang, M. Ma, J. Zhang, H. Wen, D. Zheng and Y. Yao, *Chem. Commun.*, 2018, **54**, 9234-9237.
4. T. Yang, J. Liang, I. Sultana, M. M. Rahman, M. J. Monteiro, Y. Chen, Z. Shao, S. R. P. Silva and J. Liu, *J. Mater. Chem. A*, 2018, **6**, 8280-8288.
5. Q. Liu, H. Shi, T. Yang, Y. Yang, Z.-S. Wu, J. Yu, S. R. P. Silva and J. Liu, *J. Mater. Chem. A*, 2019, **7**, 6197-6204.
6. P. Ratajczak, M. E. Suss, F. Kaasik and F. Béguin, *Energy Storage Mater.*, 2018, **16**, 126-145.
7. P. Lu, X. Wang, L. Wen, X. Jiang, W. Guo, L. Wang, X. Yan, F. Hou, J. Liang, H. M. Cheng and S. X. Dou, *Small*, 2019, **15**.
8. T. Yang, R. Zhou, D. W. Wang, S. P. Jiang, Y. Yamauchi, S. Z. Qiao, M. J. Monteiro and J. Liu, *Chem. Commun.*, 2015, **51**, 2518-2521.
9. F. Wang, X. Wu, X. Yuan, Z. Liu, Y. Zhang, L. Fu, Y. Zhu, Q. Zhou, Y. Wu and W. Huang, *Chem. Soc. Rev.*, 2017, **46**, 6816-6854.
10. Y. Wang, X. Fu, M. Zheng, W. H. Zhong and G. Cao, *Adv. Mater.*, 2019, **31**, 1804204 -1804233
11. G. Zhu, H. Wen, M. Ma, W. Wang, L. Yang, L. Wang, X. Shi, X. Cheng, X. Sun and Y. Yao, *Chem. Commun.*, 2018, **54**, 10499-10502.
12. Y. Zeng, Y. Han, Y. Zhao, Y. Zeng, M. Yu, Y. Liu, H. Tang, Y. Tong and X. Lu, *Adv. Energy Mater.*, 2015, **5**, 1402176.
13. X. Cao, B. Zheng, W. Shi, J. Yang, Z. Fan, Z. Luo, X. Rui, B. Chen, Q. Yan and H. Zhang, *Adv. Mater.*, 2015, **27**, 4695-4701.
14. Y. Wang and G. Z. Cao, *Chem. Mater.*, 2006, **18**, 2787-2804.
15. M. Ghosh, V. Vijayakumar, R. Soni and S. Kurungot, *Nanoscale*, 2018, **10**, 8741-8751.
16. T. Zhai, S. Xie, M. Yu, P. Fang, C. Liang, X. Lu and Y. Tong, *Nano Energy*, 2014, **8**, 255-263.
17. H. S. Kim, J. B. Cook, H. Lin, J. S. Ko, S. H. Tolbert, V. Ozolins and B. Dunn, *Nat. Mater.*, 2017, **16**, 454-460.
18. S. Yang, Y. Liu, Y. Hao, X. Yang, W. A. Goddard, 3rd, X. L. Zhang and B. Cao, *Adv. Sci.*, 2018, **5**, 1700659-1700669.
19. Y. Lv, Z. Chen, Y. Liu, T. Wang and Z. Ming, *Nano-Structures & Nano-Objects*, 2018, **15**, 114-118.
20. C. X. Guo, G. Yilmaz, S. Chen, S. Chen and X. Lu, *Nano Energy*, 2015, **12**, 76-87.
21. T. Qian, N. Xu, J. Q. Zhou, T. Z. Yang, X. J. Liu, X. W. Shen, J. Q. Liang and C. L. Yan, *J. Mater. Chem. A*, 2015, **3**, 488-493.
22. F. Huguenin, M. Ferreira, V. Zucolotto, F. C. Nart, R. M. Torresi and O. N. Oliveira, *Chem. Mater.*, 2004, **16**, 2293-2299.
23. W. Bi, Y. Wu, C. Liu, J. Wang, Y. Du, G. Gao, G. Wu and G. Cao, *ACS Appl. Energy Mater.*, 2018, **2**, 668-677.
24. W. Bi, E. P. Jahrman, G. T. Seidler, J. Wang, G. Gao, G. Wu, M. Atif, M. S. AlSalhi and G. Cao, *ACS Appl. Mater. Interfaces*, 2019, **11** 16647-16655.
25. G. T. Seidler, D. R. Mortensen, A. J. Remesnik, J. I. Pacold, N. A. Ball, N. Barry, M. Styczinski and O. R. Hoidn, *Rev. Sci. Instrum.*, 2014, **85**, 113906.

26. E. P. Jahrman, W. M. Holden, A. S. Ditter, D. R. Mortensen, G. T. Seidler, T. T. Fister, S. A. Kozimor, L. F. J. Piper, J. Rana, N. C. Hyatt and M. C. Stennett, *Rev. Sci. Instrum.*, 2019, **90**, 024106-024121.
27. W. Bi, G. Gao, Y. Wu, H. Yang, J. Wang, Y. Zhang, X. Liang, Y. Liu and G. Wu, *RSC Adv.*, 2017, **7**, 7179-7187.
28. A. T. Lawal and G. G. Wallace, *Talanta*, 2014, **119**, 133-143.
29. X. W. Zhou, G. M. Wu, J. D. Wu, H. Yang, J. Wang, G. Gao, R. Cai and Q. Yan, *J. Mater. Chem. A*, 2013, **1**, 15459-15468.
30. J. G. Wang, H. Liu, H. Liu, W. Hua and M. Shao, *ACS Appl. Mater. Interfaces*, 2018, **10**, 18816-18823.
31. C. Jiang, G. Chen and X. Wang, *Synth. Met.*, 2012, **162**, 1968-1971.
32. I. Šeděnková, M. Trchová and J. Stejskal, *Polym. Degrad. Stabil.*, 2008, **93**, 2147-2157.
33. M. H. Bai, T. Y. Liu, F. Luan, Y. Li and X.-X. Liu, *J. Mater. Chem. A*, 2014, **2**, 10882-10888.
34. H. Wang, L. Bian, P. Zhou, J. Tang and W. Tang, *J. Mater. Chem. A*, 2013, **1**, 578-584.
35. P. Simon and Y. Gogotsi, *Nat. Mater.*, 2008, **7**, 845-854.
36. D. O. Scanlon, A. Walsh, B. J. Morgan and G. W. Watson, *J. Phys. Chem. C*, 2008, **112**, 9903-9911.
37. Y. Zheng, T. Zhou, X. Zhao, W. K. Pang, H. Gao, S. Li, Z. Zhou, H. Liu and Z. Guo, *Adv Mater*, 2017, **29**.
38. X. Zhao, H.-E. Wang, X. Chen, J. Cao, Y. Zhao, Z. Garbe Neale, W. Cai, J. Sui and G. Cao, *Energy Storage Materials*, 2018, **11**, 161-169.
39. H. Song, C. Liu, C. Zhang and G. Cao, *Nano Energy*, 2016, **22**, 1-10.
40. G. A. Snook, P. Kao and A. S. Best, *J. Power Sources*, 2011, **196**, 1-12.
41. Y. Li, Y. Lei, B. G. Shen and J. R. Sun, *Sci. Rep.*, 2015, **5**, 14576.
42. Y. Yan, Q. Cheng, Z. Zhu, V. Pavlinek, P. Saha and C. Li, *J. Power Sources*, 2013, **240**, 544-550.

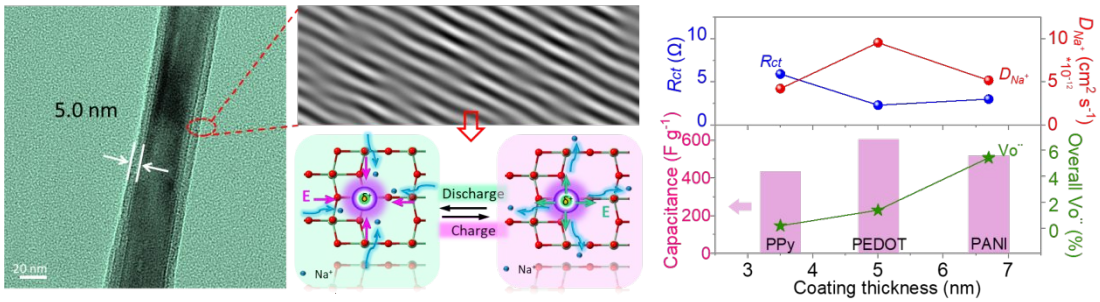

Interface oxygen vacancies contained V_2O_5 caused by various conductive polymers with built-in local electric field for high-energy supercapacitors